

## Supporting Information for

### Determination of optimum optoelectronic properties in vertically stacked

### MoS<sub>2</sub>/h-BN/WSe<sub>2</sub> van der Waals heterostructures

Shilin Tan,<sup>a</sup> Yipeng Zhao,<sup>a</sup> Jiansheng Dong,<sup>a</sup> Guowei Yang<sup>b</sup> and Gang Ouyang<sup>\*a</sup>

<sup>a</sup> *Key Laboratory of Low-Dimensional Quantum Structures and Quantum Control of Ministry of Education, Synergetic Innovation Center for Quantum Effects and Applications (SICQEA), Hunan Normal University, Changsha 410081, Hunan, China*

<sup>b</sup> *State Key Laboratory of Optoelectronic Materials and Technologies, Institute of Optoelectronic and Functional Composite Materials, Nanotechnology Research Center, School of Physics and Engineering, Sun Yat-sen University, Guangzhou 510275, Guangdong, China*

\* Corresponding author: gangouy@hunnu.edu.cn

### Theoretical details:

Considering the difference between surface and core interior of a nanosystem, the lattice strain can be expressed as:  $\langle \varepsilon \rangle = \sum_{i \leq n_s} \gamma_i (z_i c_i / z_b - 1)$ , where  $n_s$  is number of surface layer,  $z_i$ ,  $z_b$  and  $c_i = 2 / (1 + \exp((12 - z_i) / 8z_i))$  are the effective coordination numbers (CNs) of specific  $i$ th atomic layer and that of the bulk, and the bond contraction coefficient, respectively.<sup>1</sup>  $\gamma_i = \tau_0 c_i d_0 / D$  is the surface-to-volume ratio (SVR), where  $d_0$  is the bond length of Mo-S (W-Se) and B-N,  $D$  represents the thickness, and  $\tau_0$  is the dimensionality of TMD ( $\tau_0 = 2$ ) and a thin plate ( $\tau_0 = 1$ ).<sup>1-3</sup>

Furthermore, the cohesive energy of a nanosystem can be shown as:<sup>3,4</sup>  
 $E_{coh}(D) = \sum_{i \leq n_s} N_i z_i E_i + \left( N - \sum_{i \leq n_s} N_i \right) E_b$ , because the sum of single-bond energy ( $E_b$ ) of an atom with all nearest neighbors can be approximated by its cohesive energy ( $E_{coh}$ ), i.e.,  $E_{coh} = z E_b$ , where  $z$  is the atomic CNs.<sup>5</sup>  $E_i = c_i^{-m} E_b$  is the single-bond energy of Mo-S (W-Se) and B-N in the  $i$ th surface layer owing to the surface effect,  $m$  is the bond nature factor, and  $N_i$  ( $N$ ) is the number of atoms in the  $i$ th surface layer (total atoms).<sup>1</sup> Therefore, we have

$$\Delta E_{coh}(D) / E_{coh}(\infty) = \sum_{i \leq n_s} \gamma_i \left( z_i c_i^{-m} / z_b - 1 \right) \quad (S1)$$

Physically, the width of bandgap ( $E_g$ ) from the crystal potential is proportional to first Fourier coefficient of the entire crystal potential energy,<sup>4,5</sup> i.e.,  $E_g \propto \langle E_0 \rangle = E_{coh} / N \langle z \rangle$ , where  $\langle z \rangle = \sum_{i \leq n_s} \gamma_i (z_i - z_b) + z_b$  is the average CNs. Consequently, we obtain the size-dependent bandgap from the above relationships

$$E_g(D) = \frac{z_b}{\langle z \rangle} \left[ \sum_{i \leq n_s} \gamma_i \left( \frac{z_i}{z_b} c_i^{-m} - 1 \right) + 1 \right] E_g(\infty) \quad (S2)$$

where  $E_g(\infty)$  denotes the bandgap energy of bulk.

In addition, in the light of size-dependent shifts of conduction band minimum (CBM) and valence band maximum (VBM) deduced by Brus<sup>6</sup> and Colvin,<sup>7</sup>  $\Delta E_{\text{CBM}}(D) = \hbar^2 \pi^2 / 2m_e D^2$  and  $\Delta E_{\text{VBM}}(D) = \hbar^2 \pi^2 / 2m_h D^2$ , respectively, and combined with thermodynamic method,<sup>8</sup> the size-dependent shifts of CBM and VBM are

$$\begin{cases} \Delta E_{\text{CBM}}(D) = \frac{z_b E_{\text{coh}} / \langle z \rangle E_{\text{coh}}(\infty) - 1}{m_e / m_h + 1} E_g(\infty) \\ \Delta E_{\text{VBM}}(D) = \frac{z_b E_{\text{coh}} / \langle z \rangle E_{\text{coh}}(\infty) - 1}{m_h / m_e + 1} E_g(\infty) \end{cases} \quad (\text{S3})$$

where  $m_e$  and  $m_h$  are the effective mass of electron and hole, and  $\hbar$  is the reduced Planck constant. Meanwhile, the barrier height defined by the band offset at a heterointerface has an effect on the interlayer recombination and photocarrier collection, thus we need to analyze the conduction band offset (CBO)  $\Delta E_c$  and valence band offset (VBO)  $\Delta E_v$  at the heterointerface by work function and electron affinities, i.e.,

$$\begin{cases} \Delta E_c = \chi_i - \chi_2 \\ \Delta E_v = \Delta E_g - \Delta E_c \end{cases} \quad (\text{S4})$$

where  $\chi_i$  is the electron affinity of MoS<sub>2</sub> and WSe<sub>2</sub>,  $\chi_2$  is the electron affinity of h-BN,  $\chi = \chi^B - \Delta E_{\text{CBM}}(D)$ ,  $\Delta E_g$  is the bandgap difference between h-BN and MoS<sub>2</sub> (WSe<sub>2</sub>), and the electron affinity in the bulk is  $\chi^B = \chi^{\text{monolayer}} + \Delta E_{\text{CBM}}(\text{monolayer})$ .

Figure S1a shows the size-dependent cohesive energy of MoS<sub>2</sub> (WSe<sub>2</sub>) and h-BN. Clearly, the change trend of cohesive energy of h-BN is smaller than that of MoS<sub>2</sub> (WSe<sub>2</sub>). It should be related to the structure of the material, h-BN is a planar hexagonal structure semiconductor, the change of energy in multilayer h-BN is mainly provided by vdW force, and the relaxation of chemical bonds in the plane is

small, but the intralayer chemical bonds of the sandwich-structure TMDs has a large relaxation after stacking multilayer TMDs.

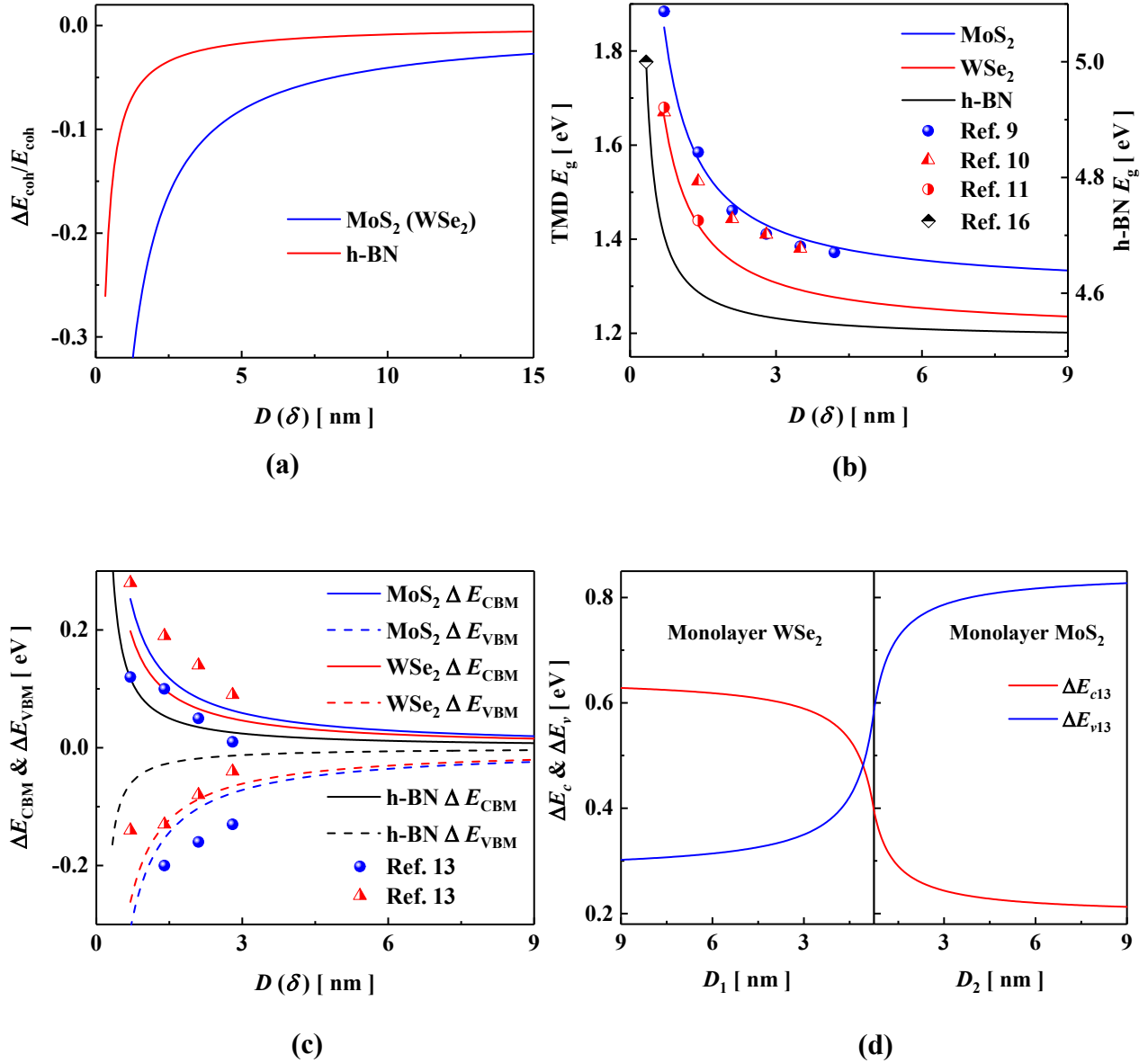
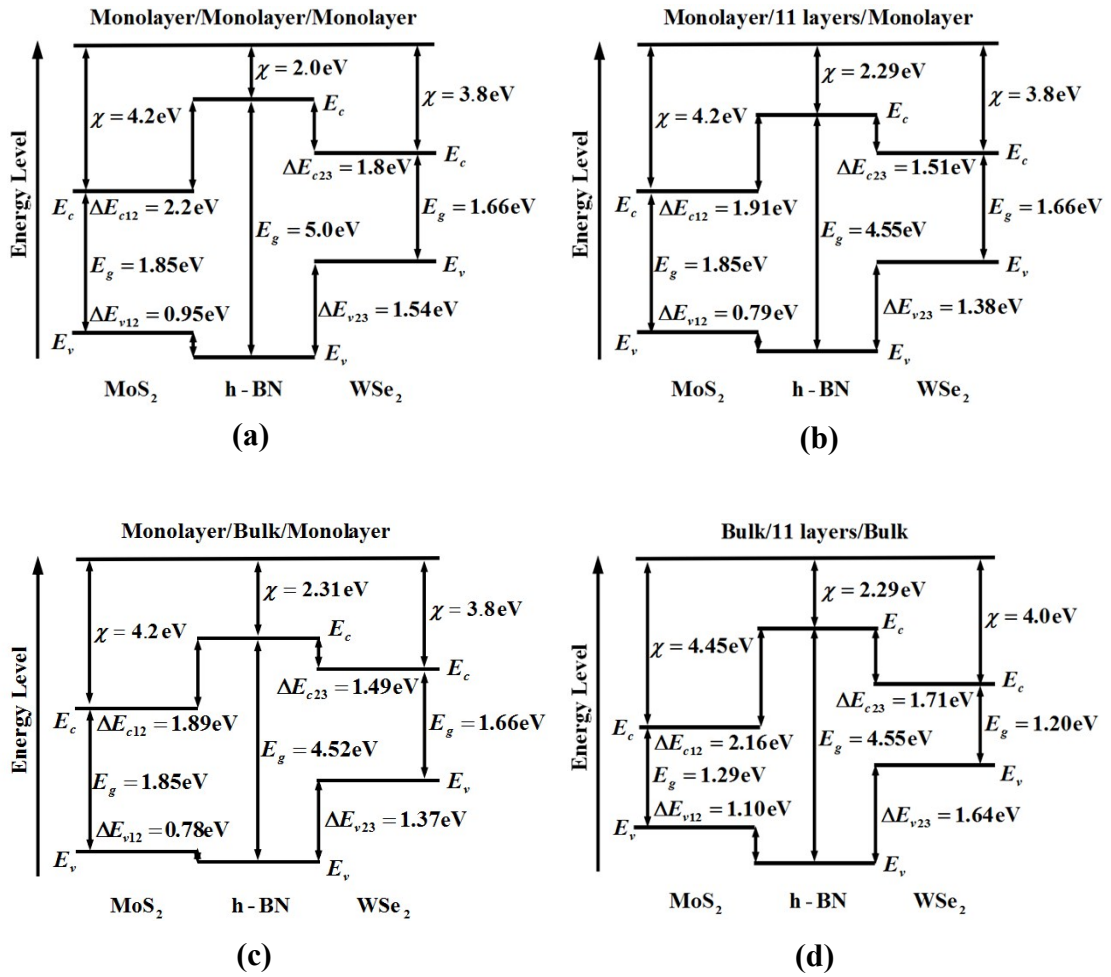


**Figure S1.** (a) Dependence of a relative change of cohesive energy on thickness. (b) Size-dependent bandgap, (c) band shift of MoS<sub>2</sub>, WSe<sub>2</sub> and h-BN. (d) MoS<sub>2</sub> thickness-dependent CBO and VBO between MoS<sub>2</sub> and monolayer WSe<sub>2</sub> (Left), and WSe<sub>2</sub> thickness-dependent CBO and VBO between monolayer MoS<sub>2</sub> and WSe<sub>2</sub> (Right).

In addition, the cohesive energy decreases with decreasing thickness of TMD (h-BN), this trend is mainly related to the CN imperfection and the SVR that decrease with increasing thickness. As the size decreases, the surface effect of bond-order loss and the less-CN's will induce the bond spontaneous shrinkage, resulting in system relaxation into a new self-equilibrium state. Therefore, the bandgap of MoS<sub>2</sub>, WSe<sub>2</sub> and h-BN shows a significant redshift with increasing thickness (Fig.S1b). Our results agree reasonably well with the experimental observations and DFT calculations.<sup>9-11</sup> Moreover, it has been reported that the binding energy of interlayer excitons decreases with increasing of h-BN thickness or vacuum between MoS<sub>2</sub> and WSe<sub>2</sub> while the binding energy of intralayer excitons remains constant in MoS<sub>2</sub>/h-BN/WSe<sub>2</sub>.<sup>12</sup>

Figure S1c shows the size-dependent band-edge shifts of MoS<sub>2</sub>, WSe<sub>2</sub> and h-BN. Clearly, as the thickness decreases, the shifts of CBM and VBM increase, that is, the conduction band energy increases and the valence band energy decreases. The trend is related to the cohesive energy of system and can be attributed to the repulsion between cation *d* orbital and anion *p* orbital for TMDs.<sup>13</sup> Meanwhile, we obtain band offsets at MoS<sub>2</sub>-WSe<sub>2</sub> interface (Fig.S1d). Evidently, the CBO between MoS<sub>2</sub> and WSe<sub>2</sub> in monolayer WSe<sub>2</sub> (MoS<sub>2</sub>) increases with increasing (decreasing) thickness of MoS<sub>2</sub> (WSe<sub>2</sub>), whereas the VBO in monolayer WSe<sub>2</sub> (MoS<sub>2</sub>) decreases as the thickness of MoS<sub>2</sub> (WSe<sub>2</sub>) increases (decreases). Physically, the conduction band energy decreases and the valence band energy increases as the thickness increases,<sup>13</sup> thus this trend of CBO and VBO is exhibited in the MoS<sub>2</sub>/WSe<sub>2</sub> with type II band alignment. In addition, due to the difference of electron affinity and bandgap, and the distinct CBO and VBO at the interface, it supplies a viable approach that the band alignment can be modulated by the thickness.

Figure S2 shows the band alignment of the vertical stacked MoS<sub>2</sub>/h-BN/WSe<sub>2</sub> vdW heterostructure under different thicknesses. Obviously, regardless of the thickness of TMDs and h-BN, MoS<sub>2</sub> and WSe<sub>2</sub> can form type II band alignment, which facilitate the separation of photogenerated carriers to reduce intralayer radiation recombination, and h-BN forms type I band alignment with MoS<sub>2</sub> and WSe<sub>2</sub>.



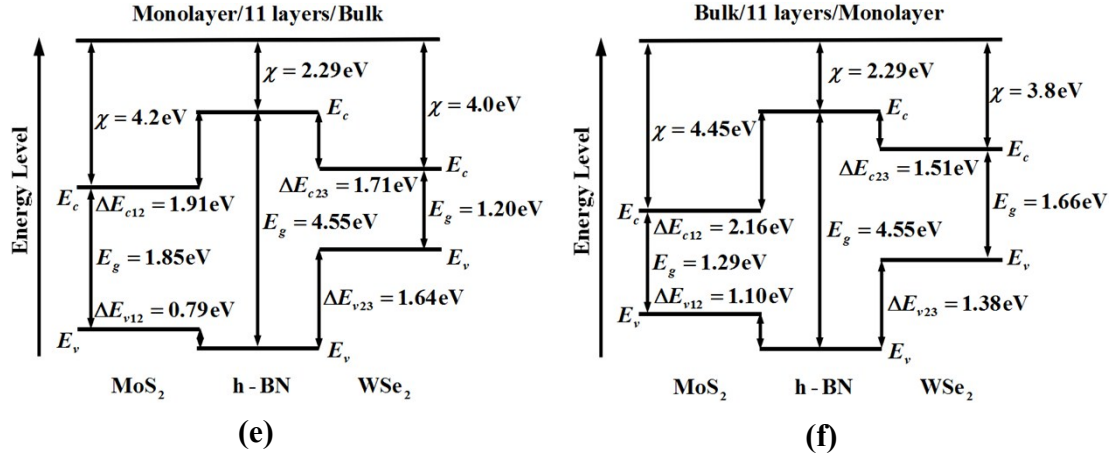


**Figure S2.** Band alignment of MoS<sub>2</sub>/h-BN/WSe<sub>2</sub> with different configurations, (a) monolayer/monolayer/monolayer, (b) monolayer/11-layers/monolayer, (c) monolayer/bulk/monolayer, (d) bulk/11-layers/bulk, (e) monolayer/11-layers/bulk, and (f) bulk/11-layers/monolayer, respectively.

Besides, the VBO ( $\Delta E_v$ ) at h-BN/MoS<sub>2</sub> interface is small ( $< 0.78$  eV), and the CBO ( $\Delta E_c$ ) at h-BN/MoS<sub>2</sub> interface is larger ( $> 1.89$  eV). It is expected that the intercalated h-BN has less influence on the hole current and can suppress the transfer of electrons from n-type MoS<sub>2</sub> to p-type WSe<sub>2</sub> to reduce the interlayer recombination. This special type band alignment makes the h-BN have the characteristics of electron-blocking/hole-transporting and can improve the photoelectric conversion, which has been verified in some experiments.<sup>14-17</sup> Otherwise, the band alignment at different thicknesses reveals that the electron affinity and ionization energy of MoS<sub>2</sub>, WSe<sub>2</sub> and h-BN are different, which supplies the theoretical support for the design of optoelectronic devices.

Figure S3a clearly shows that the PCE increases with increasing thickness of MoS<sub>2</sub> ( $D_1$ ) and WSe<sub>2</sub> ( $D_2$ ) and almost reaches maximum of 14% at  $\sim 15$  nm without h-

BN. It can be attributed to the optical absorption and bandgap, resulting in a lower threshold value of photo-generating carriers.

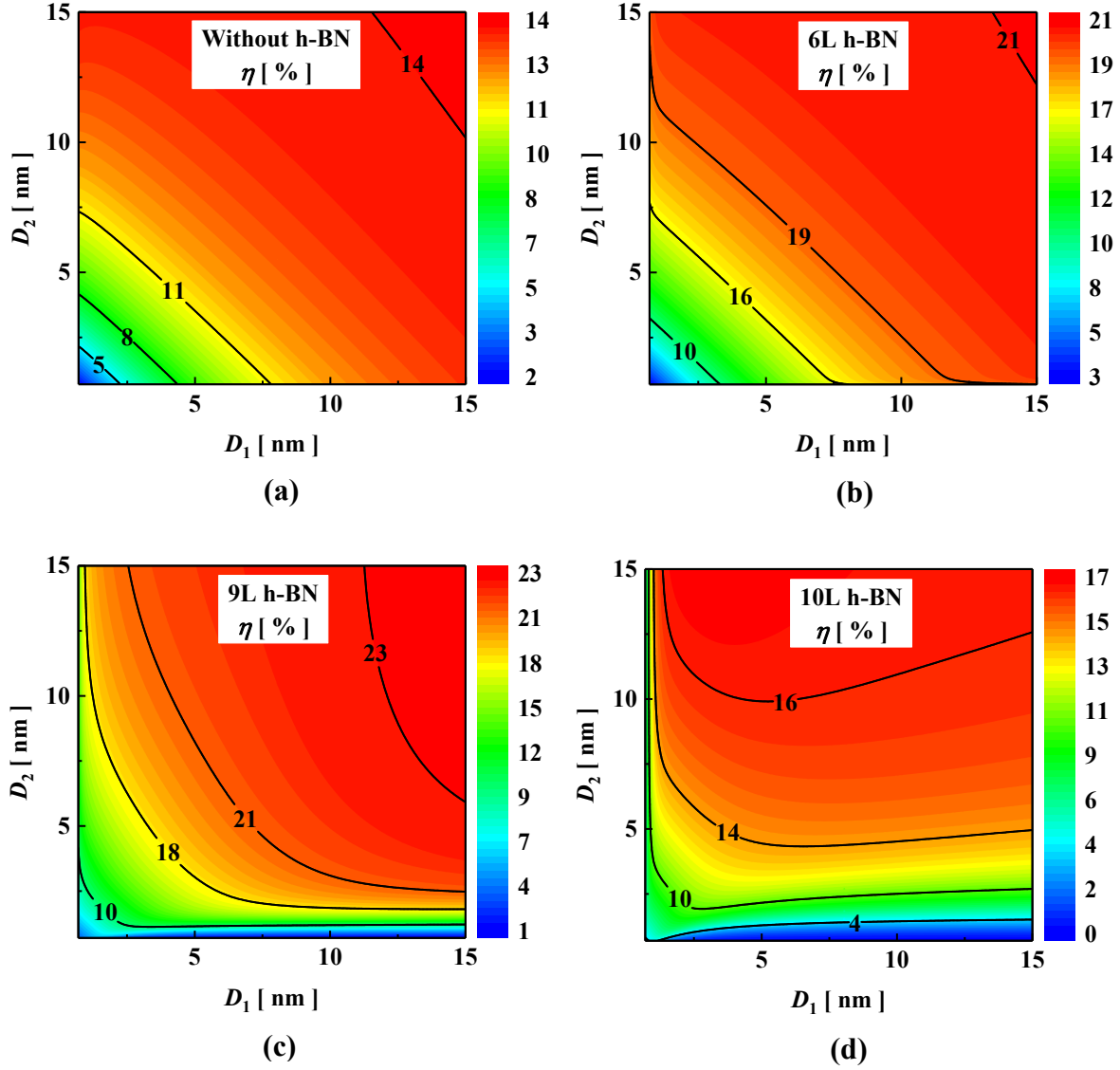


**Figure S3.** Size-dependent PCE diagram of MoS<sub>2</sub>/h-BN/WSe<sub>2</sub> under different intercalated layers, (a) 0L, (b) 6-layers, (c) 9-layers, (d) 10-layers.

Current measurements of  $V_{oc}$  in the MoS<sub>2</sub>/WSe<sub>2</sub> heterostructure solar cells is 0.2-0.3 V, and the PCEs are about 0.2% and 0.4%,<sup>18-20</sup> which is much lower than predicted, mainly due to the inferior  $V_{oc}$  of the system caused by surface contact,

impurity concentration and defects. Figure S3b, 3c and 3d depict the PCE under 6, 9 and 10 h-BN layers as a function of  $D_1$  and  $D_2$ . Evidently, the PCE has a maximum of 23.24% under 9-layers h-BN, which is nearly twice that of without h-BN. And the PCE is reduced in the case of 10-layers h-BN, which can be attributed to the suppression of carrier collection. In addition, when the thickness of h-BN is >6-layers and the thickness of MoS<sub>2</sub> (WSe<sub>2</sub>) is maintained at a certain value, the negative effect of intercalated h-BN on photoelectric conversion of multilayer/few-layer (few-layer/multilayer) MoS<sub>2</sub>/WSe<sub>2</sub> is more obvious as the thickness of WSe<sub>2</sub> (MoS<sub>2</sub>) increases. The physical origin is that the  $\Delta E_{c13}$  ( $\Delta E_{v13}$ ) between MoS<sub>2</sub> and WSe<sub>2</sub> decreases as the thickness of WSe<sub>2</sub> (MoS<sub>2</sub>) increases (Fig. S1d), which can weaken the photocarrier transport. Therefore, in order to enhance the photoelectric conversion of MoS<sub>2</sub>/WSe<sub>2</sub> vdW heterostructure, it is a feasible method to introduce a dielectric layer at the heterointerface to reduce interlayer recombination.

**Table S1.** The parameters in our calculations are listed as: monolayer thickness  $D$  ( $\delta$ ), Mo-S (W-Se) and B-N bond length  $d_0$ , the effective mass of electron ( $m_e$ ) and hole ( $m_h$ ), electron affinity of single-layer material ( $\chi$ ), radiative lifetime of the excitons ( $\tau_r$ ), and surface recombination velocity ( $S_{00}$ ). Note that the  $S_{00}$  is indirectly obtained by  $S_{00} = \sqrt{D_L/\tau_L}$ , where  $D_L$  and  $\tau_L$  are the hot carrier diffusion coefficient and the carrier lifetime, respectively.

material	$D$ (nm)	$d_0$ (nm)	$m_e$ ( $m_0$ )	$m_h$ ( $m_0$ )	$\chi$ (eV)	$S_{00}$ (cm/s)	$\tau_r$ (ns)
MoS <sub>2</sub>	0.65 <sup>3</sup>	0.241 <sup>13</sup>	0.46 <sup>21</sup>	0.56 <sup>21</sup>	4.2 <sup>3</sup>	3.5×10 <sup>422</sup>	1.16 <sup>23</sup>
WSe <sub>2</sub>	0.65 <sup>3</sup>	0.255 <sup>13</sup>	0.34 <sup>21</sup>	0.44 <sup>21</sup>	3.4-4.0 <sup>3</sup>	1.0×10 <sup>724</sup>	4.0 <sup>25</sup>
h-BN	0.33 <sup>26</sup>	0.250 <sup>27</sup>	0.26 <sup>28</sup>	0.50 <sup>28</sup>	2.0-2.3 <sup>28</sup>	—	—

**Table S2.** Calculated photoelectric parameters of MoS<sub>2</sub>/h-BN/WSe<sub>2</sub> vdW heterostructures under different cases. The bandgap of monolayer h-BN is 5.0 eV, and  $\xi/k_b T_c = 2.49\text{nm}^{-1}$  is obtained by using the Eq. (5) from Ref. (16) under different h-BN thickness.

Monolayer TMDs	$J_{sc}$ [mA/cm <sup>2</sup> ]	$V_{oc}$ [V]	PCE [%]	$FF$ [%]
MoS <sub>2</sub> /WSe <sub>2</sub>	3.56	0.58	1.70	82.4
MoS <sub>2</sub> -h-BN(1L)-WSe <sub>2</sub>	3.52	0.65	1.89	83.2
MoS <sub>2</sub> -h-BN(7L)-WSe <sub>2</sub>	3.25	1.01	2.78	84.7
MoS <sub>2</sub> -h-BN(10L)-WSe <sub>2</sub>	3.12	1.19	3.15	84.8
MoS <sub>2</sub> -h-BN(11L)-WSe <sub>2</sub>	3.04	1.25	3.23	85.0
MoS <sub>2</sub> -h-BN(12L)-WSe <sub>2</sub>	2.73	1.31	3.03	84.7
MoS <sub>2</sub> -h-BN(13L)-WSe <sub>2</sub>	1.50	1.36	1.72	84.3
MoS <sub>2</sub> -h-BN(14L)-WSe <sub>2</sub>	0.30	1.34	0.34	83.9
MoS <sub>2</sub> -h-BN(15L)-WSe <sub>2</sub>	0.04	1.28	0.04	78.1

## References

- 1 C. Q. Sun, *Prog. Solid State Chem.*, 2007, **35**, 1-159.
- 2 G. Ouyang, C. X. Wang and G. W. Yang, *Chem. Rev.*, 2009, **109**, 4221-4247.
- 3 Y. Zhao, W. Yu and G. Ouyang, *J. Phys. D: Appl. Phys.*, 2017, **51**, 015111.
- 4 Z. M. Zhu, A. Zhang, G. Ouyang and G. W. Yang, *Appl. Phys. Lett.*, 2011, **98**, 263112.
- 5 G. Ouyang, W. G. Zhu, C. Q. Sun, Z. M. Zhu and S. Z. Liao, *Phys. Chem. Chem. Phys.*, 2010, **12**, 1543-1549.
- 6 L. Brus, *J. Phys. Chem.*, 1986, **90**, 2555-2560.
- 7 V. L. Colvin, A. P. Alivisatos and J. G. Tobin, *Phys. Rev. Lett.*, 1991, **66**, 2786-2789.
- 8 Y. F. Zhu and Q. Jiang, *Coord. Chem. Rev.*, 2016, **326**, 1-33.
- 9 K. F. Mak, C. Lee, J. Hone, J. Shan and T. F. Heinz, *Phys. Rev. Lett.*, 2010, **105**, 136805.
- 10 W. Zhao, Z. Ghorannevis, L. Chu, M. Toh, C. Kloc, P.-H. Tan and G. Eda, *ACS Nano*, 2012, **7**, 791-797.
- 11 W. S. Yun, S. W. Han, S. C. Hong, I. G. Kim and J. D. Lee, *Phys. Rev. B*, 2012, **85**, 033305.
- 12 S. Latini, K. T. Winther, T. Olsen and K. S. Thygesen, *Nano Lett.*, 2017, **17**, 938-945.
- 13 J. Kang, S. Tongay, J. Zhou, J. Li and J. Wu, *Appl. Phys. Lett.*, 2013, **102**, 012111.
- 14 J.-H. Meng, X. Liu, X.-W. Zhang, Y. Zhang, H.-L. Wang, Z.-G. Yin, Y.-Z. Zhang, H. Liu, J.-B. You and H. Yan, *Nano Energy*, 2016, **28**, 44-50.
- 15 S. Lin, X. Li, P. Wang, Z. Xu, S. Zhang, H. Zhong, Z. Wu, W. Xu and H. Chen, *Sci. Rep.*, 2015, **5**, 15103.

- 16 Q. A. Vu, J. H. Lee, V. L. Nguyen, Y. S. Shin, S. C. Lim, K. Lee, J. Heo, S. Park, K. Kim, Y. H. Lee and W. J. Yu, *Nano Lett.*, 2017, **17**, 453-459.
- 17 X. Li, S. Lin, X. Lin, Z. Xu, P. Wang, S. Zhang, H. Zhong, W. Xu, Z. Wu and W. Fang, *Optics Express*, 2016, **24**, 134-145.
- 18 M. M. Furchi, A. Pospischil, F. Libisch, J. Burgdörfer and T. Mueller, *Nano Lett.*, 2014, **14**, 4785-4791.
- 19 M. M. Furchi, A. A. Zechmeister, F. Hoeller, S. Wachter, A. Pospischil and T. Mueller, *IEEE J. Sel. Top. Quantum Electron.*, 2017, **23**, 106-116.
- 20 J. Wong, D. Jariwala, G. Tagliabue, K. Tat, A. R. Davoyan, M. C. Sherrott and H. A. Atwater, *ACS Nano*, 2017, **11**, 7230-7240.
- 21 S. Das, A. Prakash, R. Salazar and J. Appenzeller, *ACS Nano*, 2014, **8**, 1681-1689.
- 22 P. Yuan, J. Liu, R. Wang and X. Wang, *Nanoscale*, 2017, **9**, 6808-6820.
- 23 T. Huang, P. Han, X. Wang, J. Ye, W. Sun, S. Feng and Y. Zhang, *J. Phys. D: Appl. Phys.*, 2017, **50**, 114005.
- 24 M. S. Eggleston, S. Desai, K. Messer, S. Madhvapathy, J. Xiao, X. Zhang, E. Yablonovitch, A. Javey and M. C. Wu, *CLEO: QELS\_Fundamental Science. Optical Society of America*, 2015, FTu1E. 5.
- 25 C. Jin, J. Kim, K. Wu, B. Chen, E. S. Barnard, J. Suh, Z. Shi, S. G. Drapcho, J. Wu, P. J. Schuck, S. Tongay and F. Wang, *Adv. Funct. Mater.*, 2017, **27**, 1601741.
- 26 C. Zhang, L. Fu, S. Zhao, Y. Zhou, H. Peng and Z. Liu, *Adv. Mater.*, 2014, **26**, 1776-1781.
- 27 J. Wang, F. Ma, W. Liang, R. Wang and M. Sun, *Nanophotonics*, 2017, **6**, 943-976.
- 28 M. S. Choi, G.-H. Lee, Y.-J. Yu, D.-Y. Lee, S. H. Lee, P. Kim, J. Hone and W. J. Yoo, *Nat. Commun.*, 2013, **4**, 1624.